Impedance spectroscopy studies on (Na0.5Bi0.5)0.94Ba0.06TiO3 + 0.3 wt% Sm2O3 + 0.25 wt% LiF lead-free piezoelectric ceramics

N. Zidi, Ahcène Chaouchi, Sophie d'Astorg, Mohamed Rguiti, Christian Courtois

Bull. Mater. Sci., Vol. 38, No. 3, June 2015, pp. 731–737. © Indian Academy of Sciences.

Impedance spectroscopy studies on $(Na_{0.5}Bi_{0.5})_{0.94}Ba_{0.06}TiO_3 + 0.3$ wt% $Sm_2O_3 + 0.25$ wt% LiF lead-free piezoelectric ceramics

N ZIDI[1], A CHAOUCHI[1,*], S D'ASTORG[2,3], M RGUITI[2,3] and C COURTOIS[2,3]

[1]Laboratoire de Chimie Appliquée et Génie Chimique de l'Université Mouloud Mammeri de Tizi-Ouzou, Tizi-Ouzou, Algeria

[2]Laboratoire des Matériaux Céramiques et Procédés Associés – Université de Valenciennes et du Hainaut-Cambrésis, Z.I. du Champ de l'Abbesse, 59600 Maubeuge, France

[3]Université Lille Nord de France, F-59000 Lille, France

MS received 3 February 2014; revised 14 April 2014

Abstract. **The a.c. complex impedance spectroscopy technique was used to obtain the electrical parameters of $(Na_{0.5}Bi_{0.5})_{0.94}Ba_{0.06}TiO_3 + 0.3$ wt% $Sm_2O_3 + 0.25$ wt% LiF lead-free ceramics in a wide frequency range at different temperatures. These samples were prepared by a high-temperature solid-state reaction technique and their single phase formation was confirmed by the X-ray diffraction technique. Dielectric studies exhibit a diffuse phase transition characterized by a temperature and frequency dispersion of permittivity, and this relaxation has been modelled using the modified Curie–Weiss law. The variation of imaginary part (Z'') of impedance with frequency at various temperatures shows that the Z'' values reach a maxima peak (Z''_{max}) above 400°C. The appearance of single semicircle in the Nyquist plots (Z'' *vs.* Z') pattern at high temperatures suggests that the electrical process occurring in the material has a relaxation process possibly due to the contribution for bulk material only. The bulk resistance of the material decreases with rise in temperatures similar to that of a semiconductor, and the Nyquist plot showed the negative temperature coefficient of resistance (NTCR) character of these materials. The frequencies, thermal effect on a.c. conductivity and activation energy have been assessed.**

Keywords. **$(Na_{0.5}Bi_{0.5})_{0.94}Ba_{0.06}TiO_3$; low sintering; impedance spectroscopy; dielectric relaxation; conductivity.**

1. Introduction

Lead-based ceramics have been widely used for electronic and microelectronic devices because of their excellent piezoelectric properties.[1,2] However, on account of the high volatilization of toxic lead oxide during sintering process, a great many countries have enacted laws to restrict their applications. In recent decades, more and more research works have been focused on searching for environment-friendly lead-free piezoelectric ceramics to replace the conventional lead-based materials.

$(Bi_{0.5}Na_{0.5})_{0.94}Ba_{0.06}TiO_3$ ceramics were regarded as a piezoelectric ceramics with good properties owing to the existence of a rhombohedral–tetragonal morphotropic phase boundary (MPB).[3,4] In recent times, rare earth oxide, Sm_2O_3, has been used to further improve piezoelectric properties of $(Bi_{0.5}Na_{0.5})_{0.94}Ba_{0.06}TiO_3$ ceramics,[5] and the ceramics doped with 0.3 wt% Sm_2O_3 show quite good performance with excellent piezoelectric properties (piezoelectric constant d_{33} of 202 pC N^{-1}, planar coupling factor k_p of 0.30 and mechanical quality factor Q_m of 101) and improved dielectric properties (relative dielectric constant ε_r of 2018 and dissipation factor tan δ of 0.056).

A prime requirement for the miniaturization in many systems is low sintering temperature, and this is particularly true for multilayered structures where silver is the intended electrode material. However, the high sintering temperature of these ceramics approximately 1200°C necessitates the use of expensive Ag–Pd metal for the electrode rather than cheap Ag for application to multilayer devices. On other hand, the low temperature sintering has an additional advantage in the case of lead-free piezoceramics, because they normally contain highly volatile elements such as Na, K and Bi. To reduce the sintering temperature of dielectric materials, many dopants have been employed as sintering aids, such as Li_2CO_3,[6] B_2O_3,[7] CuV_2O_6[8] and ZnBO.[9]

Generally, the addition of dopants changes the shape and growth rate of the grain in the ceramics, and their low-temperature behaviour is often controlled by grain boundaries and therefore the knowledge of behaviour of grain boundary is important.

It is also well known that the interior defects such as A-site vacancies, space charge electrons or oxygen vacancies have great influence on ferroelectric fatigue or ionic conductivity of the material.[10–13] We find that it is very important to gain a fundamental understanding of their conductive mechanism. Various kinds of defects are always suggested as being responsible for the dielectric relaxations at high temperature range.

*Author for correspondence (ahchaouchi@yahoo.fr)

The a.c. impedance analysis is a powerful means to separate out the grain boundary and grain-electrode effects, which usually are the sites of trap for defects. It is also useful in establishing its relaxation mechanism by appropriately assigning different values of resistance and capacitance to the grain and grain boundary effects.

In this paper, a detailed analysis of dielectric relaxation and a.c. impedance spectroscopy has been carried out to characterize the dielectric and conductivity properties of $(Na_{0.5}Bi_{0.5})_{0.94}Ba_{0.06}TiO_3 + 0.3$ wt% $Sm_2O_3 + 0.25$ wt% LiF in order to gain insight into the relaxation mechanism and defects relation.

2. Background

The a.c. impedance is a non-destructive experimental technique for the characterization of microstructural and electrical properties of some electronic materials. The technique is based on analysing the a.c. response of a system to a sinusoidal perturbation and subsequent calculation of impedance as a function of the frequency of the perturbation. The analysis of the electrical properties (conductivity, dielectric constant, loss, etc.) carried out using relaxation frequency (ω_{max}) values gives unambiguous results when compared with those obtained at arbitrarily selected fixed frequencies. The frequency-dependent properties of a material can be described as complex permittivity (ε^*), complex impedance (Z^*), complex admittance (Y^*), complex electric modulus (M^*) and dielectric loss or dissipation factor (tan δ). The real (ε', Z', Y', M') and imaginary (ε'', Z'', Y'', M'') parts of the complex parameters are in turn related to one another as follows:[14,15]

$$\varepsilon^* = \varepsilon' + j\varepsilon'', \tag{1}$$

$$Z^* = Z' + jZ'' = (1/jC_0\varepsilon^*\omega), \tag{2}$$

$$Y^* = Y' + jY'' = j\omega C_0\varepsilon^*, \tag{3}$$

$$M^* = M' + jM'' = (1/\varepsilon^*) = j\omega\varepsilon_0 Z^*, \tag{4}$$

$$\tan\delta = (\varepsilon''/\varepsilon') = (M'/M'') = (Y'/Y'') = (Z'/Z''), \tag{5}$$

where $\omega = 2\pi f$ is the angular frequency, C_0 the free geometrical capacitance and $j^2 = -1$. These relations offer wide scope for a graphical analysis of the various parameters under different conditions of temperature or frequency. The useful separation of intergranular phenomena depends ultimately on the choice of an appropriate equivalent circuit to represent the sample properties.

From the microstructural point of view, a ceramic sample was composed of grains and grain boundaries, which had different resistivity (ρ) and dielectric permittivity (ε).[16] The real part (Z') and imaginary part (Z'') of the complex impedance are given by below equations

$$Z' = R_g/(1 + (\omega R_g C_g)^2) + R_{gb}/(1 + (\omega R_{gb} C_{gb})^2), \tag{6}$$

$$Z'' = \omega R_g^2 C_g/(1 + (\omega R_g C_g)^2) + \omega R_{gb}^2 C_{gb}/(1 + (\omega R_{gb} C_{gb})^2), \tag{7}$$

where R_g and C_g are, respectively, the resistance and capacitance of the grain, while R_{gb} and C_{gb} are, respectively, the resistance and capacitance of the grain boundary.

3. Experimental

The $(Na_{0.5}Bi_{0.5})_{0.94}Ba_{0.06}TiO_3 + 0.3$ wt% Sm_2O_3 compound (named NBTS) was prepared by solid-state reaction using reagent grades powders of Na_2CO_3, Bi_2O_3, $BaCO_3$, TiO_2 and Sm_2O_3 (purity > 99%). These compounds were stoichiometrically mixed using ethanol and zircon balls in a Teflon jar for 2 h. The slurry was subsequently dried and the powder was manually reground and heat treated at 850°C for 2 h in air. The powder was finally reground using the same process than before in ethanol solution for 2 h.

The mixtures NBTS + 0.25 wt% LiF were prepared by mixing the powders manually in porcelain mortar. To manufacture pellets, an organic binder (polyvinyl alcohol, 5 vol%) was manually added to the powder and disks (7 and 13 mm in diameter, 1.5 and 1 mm thickness, respectively) were shaped by uni-axial pressing under 100 MPa. The green samples were finally sintered in air at 900°C for 2 h, with heating and cooling rates of 150°C h^{-1}. The crystallized phase composition has been identified by the X-ray diffraction (XRD) technique using the Cu Kα X-ray radiation (Philips X' Pert) and the microstructures were observed using a scanning electron microscopy (SEM Philips XL'30). The bulk densities of the sintered pellets were measured by the Archimedes method. The specimens were polished and electroded with a silver paste. The dielectric and electric properties were determined using HP4284A metre *vs.* temperature (from 20 to 600°C), and the frequency range from 100 kHz to 1 MHz.

4. Results and discussion

4.1 *Phase analysis and microstructure*

Figure 1 shows the X-ray diffraction patterns of the NBTS + 0.25 wt% LiF ceramics. For the diffraction patterns, a homogeneous phase was well developed without a second phase for all the specimens, which implies that the Sm^{3+} and Li^{1+} have diffused into the ceramic's lattices to form a solid solution, with the existence of tetragonal–rhombohedral phase structure. The densification ratios ρ of the sintered samples range from 92% to 95% of the theoretical one.

4.2 *Dielectric studies*

The temperature dependence of the dielectric constant (ε_r) and dielectric loss tangent (tan δ) for the 1, 10 and 100 kHz frequency range is depicted in figure 2a. The dielectric

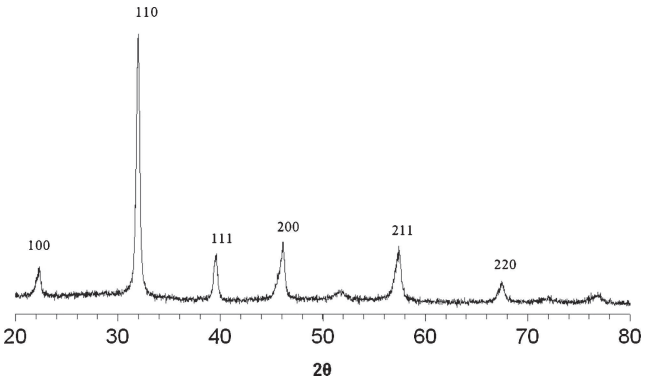

Figure 1. X-ray diffraction patterns of $(Na_{0.5}Bi_{0.5})_{0.94}Ba_{0.06}TiO_3 + 0.3$ wt% $Sm_2O_3 + 0.25$ wt% LiF composition sintered at 900°C for 2 h.

response plot exhibited a diffuse phase transition (DPT) and the temperature of the dielectric maximum (T_m) shifts towards higher temperature side with the increase in frequency which confirms the relaxor behaviour of the NBTS + 0.25 wt% LiF material. The dielectric losses (tan δ) exhibited a frequency-dependent phenomenon (figure 2a). At lower frequencies and at higher temperature the dielectrics loss shows higher values, perhaps due to the presence of the other relaxations in the materials.

The diffuse phase transition of NBTS + 0.25 wt% LiF can be described by the modified Curie–Weiss law

$$(1/\varepsilon_r) - (1/\varepsilon_m) = A(T - T_m)^\gamma, \tag{8}$$

where A is a constant and γ the diffusivity parameter.[17,18] For normal ferroelectrics γ is less than 1 and it is 1–2 for relaxor ferroelectric. Figure 2b shows the variation of $\ln((1/\varepsilon_r) - (1/\varepsilon_m))$ with $\ln(T - T_m)$ for NBTS + 0.25 wt% LiF at 100 kHz. To estimate the value of γ, the experimental data has been fitted to equation (8). The plot shows a linear behaviour with temperature and the value of γ computed to be 1.82, which clearly indicates the DPT behaviour of NBTS + 0.25 wt% LiF ceramics. It is expected that some disorder in the cation distribution (compositional fluctuations) causes the DPT where the local Curie points of different microregions statistically distribute around the mean Curie temperature.[19]

4.3 *Complex impedance spectrum analysis*

Figures 3 and 4 show the variation of the real part (Z') and imaginary part (Z'') of impedance with frequency at various temperatures, respectively.

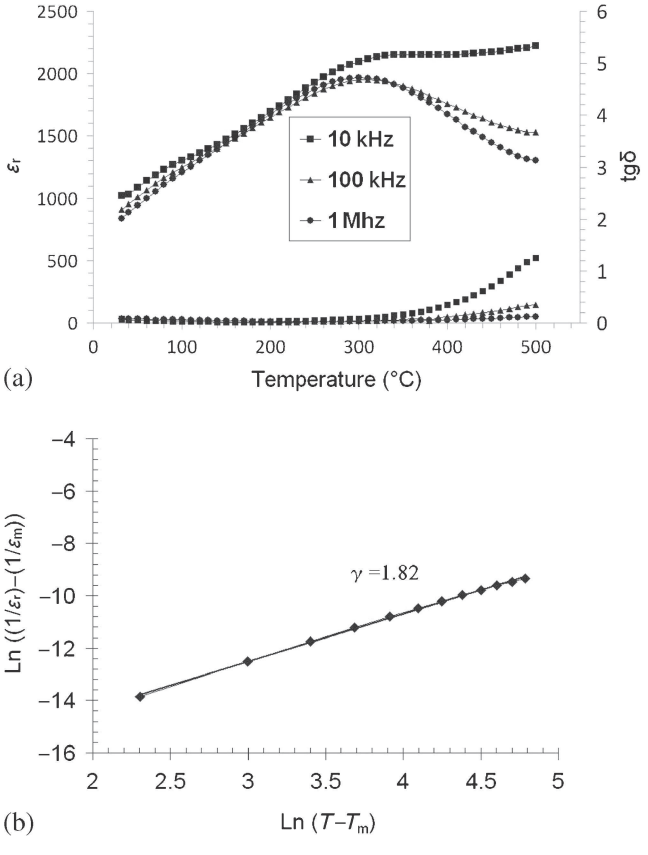

Figure 2. (**a**) Temperature dependence of permittivity and dielectric loss at different frequencies of $(Na_{0.5}Bi_{0.5})_{0.94}Ba_{0.06}TiO_3 + 0.3$ wt% $Sm_2O_3 + 0.25$ wt% LiF compositions and (**b**) plots of $\ln(1/\varepsilon_r - 1/\varepsilon_m)$ *vs.* $\ln(T - T_m)$ at 10 kHz for sintered ceramics.

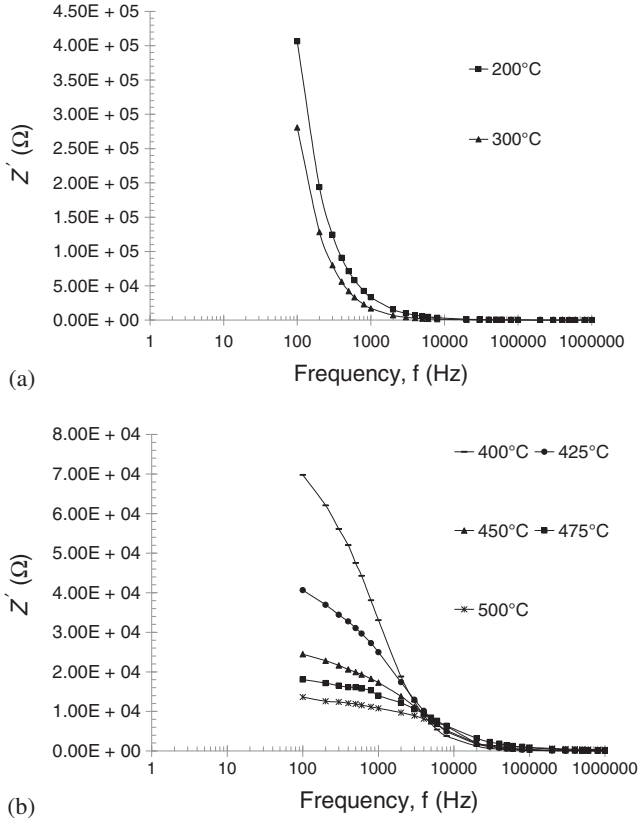

Figure 3. Variation of real part of impedance (Z') of $(Na_{0.5}Bi_{0.5})_{0.94}Ba_{0.06}TiO_3 + 0.3$ wt% $Sm_2O_3 + 0.25$ wt% LiF with frequency at different temperatures.

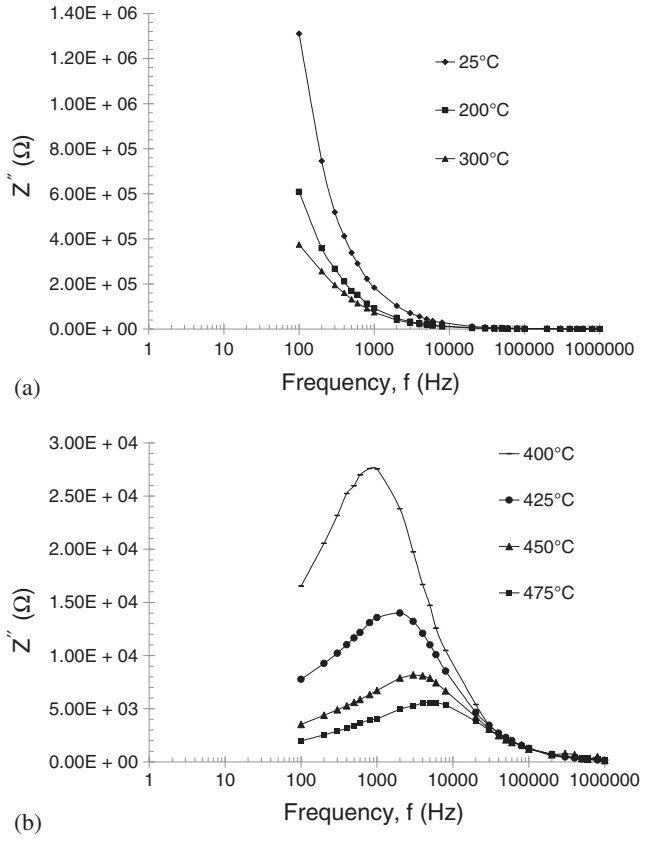

Figure 4. Variation of imaginary part (Z'') of impedance of $(Na_{0.5}Bi_{0.5})_{0.94}Ba_{0.06}TiO_3 + 0.3$ wt% $Sm_2O_3 + 0.25$ wt% LiF with frequency at different temperatures.

It is observed that the magnitude of Z' (figure 3) decreases with the increase in both frequency as well as temperature, indicating an increase in a.c. conductivity with the rise in temperature and frequency.

The merger of real part of impedance (Z') in the higher frequency domain (10 kHz) suggests a possible release of space charge and a consequent lowering of the barrier properties in the materials.[20] These phenomena may be a responsible factor for the enhancement of a.c. conductivity of material with temperature at higher frequencies. Further, at low frequencies the value of Z' decreases with the rise in temperature showing negative temperature coefficient of resistance (NTCR)-type behaviour (like that of semiconductors).

The curves (figure 4) show that the Z'' values reach a maxima peak (Z''_{max}) above 400°C (figure 4b). This pattern of variation is characterized by (i) the appearance of peaks with asymmetric broadening, (ii) shifting of the peak with decrease of the peak's height toward high frequency side on increasing temperature and (iii) the merger of spectrum in the high frequency region provides an evidence of space charge in the material that governs electrical process in the region of high frequency.[20–22] The broadening of peaks (explicit plots of Z'') suggests that, there is a spread of relaxation time (i.e., the existence of a temperature-dependent electrical relaxation phenomenon in the material.[23] Because these observations are made at higher temperatures some relaxation species, such as defects, may be responsible for electrical conduction in the material by hopping of electrons/oxygen ion vacancy/defects among the available localized sites.[20]

Figure 5 shows the curves of Z'' *vs.* Z' taken over a wide frequency range at several temperatures as a Nyquist diagram (complex impedance spectrum). It is observed that with the increase in temperature, the slope of the lines decreases and their curve bends towards real (Z') axis, and thus at temperature 400°C, a semicircle could be traced (figure 5b), indicating the increase in conductivity of the sample. The appearance of single semicircle in the impedance pattern at all temperatures suggests that the electrical process occurring in the material has a single relaxation process possibly due to the contribution for bulk material only. The centre of the semicircular arc shifts towards the origin on increasing temperature which indicates that the conductivity of the samples increases with the increase in temperature.

Figure 6 shows the normalized imaginary parts of the impedance (Z''/Z''_{max}) as a function of frequency at the selected temperatures. The curve shows peak with a slight asymmetric broadening at each temperature especially at higher temperatures. The asymmetric broadening of the peaks suggests the presence of electrical processes in the material with a spread of relaxation time.[24]

Modulus analysis is an alternative approach to explore electrical properties of the material and magnify any other effects present in the sample as a result of different relaxation time constants, and enables us to distinguish the microscopy process responsible for localized dielectric relaxations and long-range conduction.

The values (M'') components of the modulus are obtained from the following expressions:

$$M'' = \omega C_0 Z', \tag{9}$$

where C_0 is the geometrical capacitance of the empty cell.

Figure 7 shows the variation of imaginary M'' parts of the complex modulus with frequency over the entire experimental temperature range. The data presented of this way make it possible to highlight a peak which shifts in frequency with the change of temperature regarding this peak; one can conclude that the relaxation rate for this process decreases with the decrease in temperature. Let us call f_{max} the frequency corresponding to the maximum of the value of M''. For $f < f_{max}$, the charge carriers are mobile on long distances, and for $f > f_{max}$, the carriers are confined into potential wells, being mobile on short distances.

It may be mentioned here that as the NBTS sample have been synthesized at high temperature (900°C for 2 h), a slight amount of oxygen loss can occur and it may be expressed as per the Kroger–Vink notation[25]

$$O_O^X = V_{\ddot{O}} + \tfrac{1}{2}O_{2(gas)} + e'',$$

where O_O^X is the loss of lattice oxygen, $V_{\ddot{O}}$ the presence of oxygen-ion vacancy and e'' the electron released or captured.

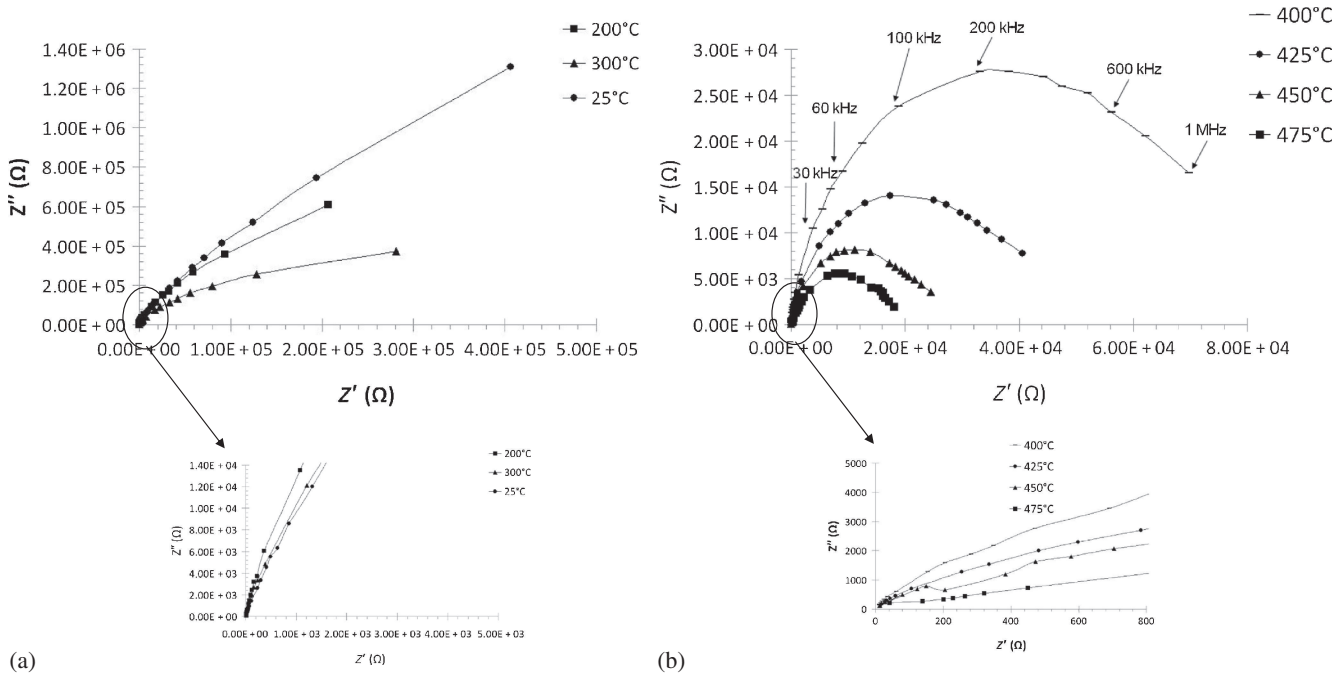

Figure 5. Complex impedance plots (Z'' *vs.* Z') of $(Na_{0.5}Bi_{0.5})_{0.94}Ba_{0.06}TiO_3 + 0.3$ wt% $Sm_2O_3 + 0.25$ wt% LiF at different temperatures.

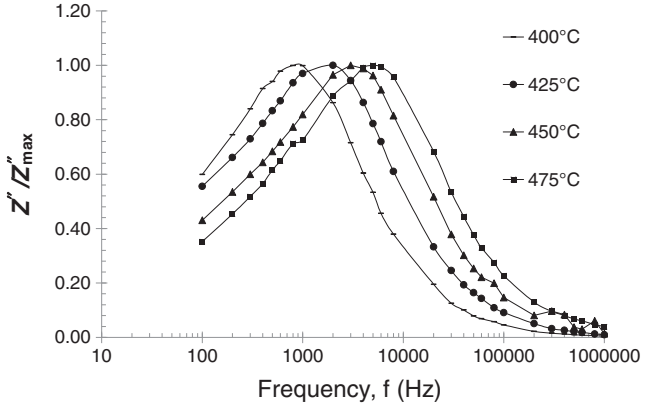

Figure 6. Normalized imaginary parts of the impedance (Z''/Z''_{max}) as a function of frequency.

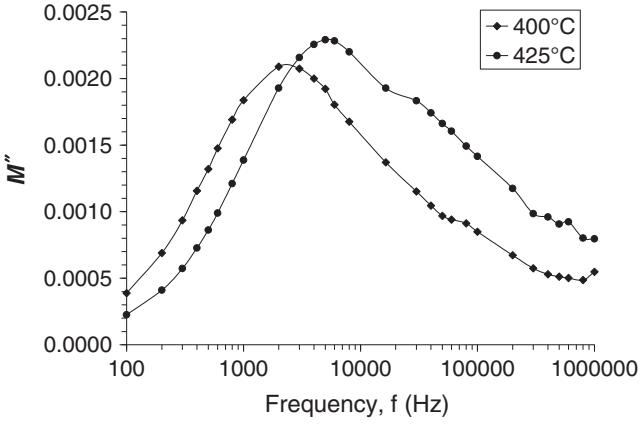

Figure 7. Variation of imaginary part of modulus M'' with frequency.

The oxygen vacancies facilitate the appearance of dipoles formed with an adjacent host ion and enlarge the rattling space available for dipole vibration, which as a consequence leads to the short-range hopping of the ions and gives rise to relaxation.

4.4 *Electrical conductivity analysis*

The a.c. electrical conductivity ($\sigma_{a.c.}$) was obtained in accordance with the following relation:

$$\sigma_{a.c.} = e/Z'S, \tag{10}$$

where e is the thickness and S the surface area of the specimen.

The $\log(\sigma_{a.c.})$ *vs.* $\log f$ plot at different temperatures (figure 8) shows a frequency-independent region in the low frequency region which corresponds to the d.c. conductivity, followed by a region which is sensitive to the frequency as well as temperature. The observed frequency-dependent conductivity can be described by this equation:

$$\sigma_{a.c.}(\omega) = \sigma_{d.c.} + A\omega^n, \tag{11}$$

where n is the frequency exponent in the range of $0 < n > 1$, A and n the thermally activated quantities, hence electrical conduction is a thermally activated process. According to Jonscher,[26] the origin of the frequency dependence of conductivity lies in the relaxation phenomena arising due to mobile charge carriers. When mobile charge carriers hop

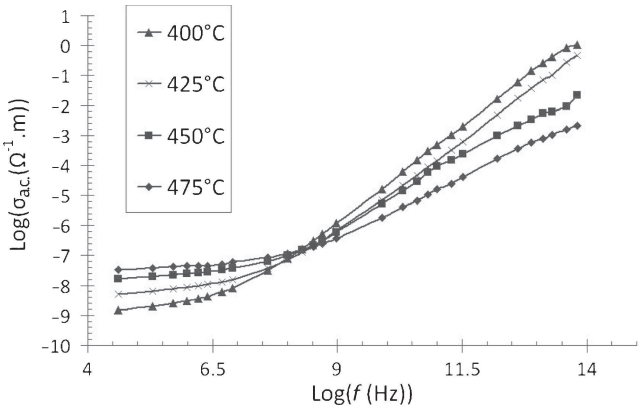

Figure 8. Frequency dependence of $\sigma_{a.c.}$ conductivity at different temperatures.

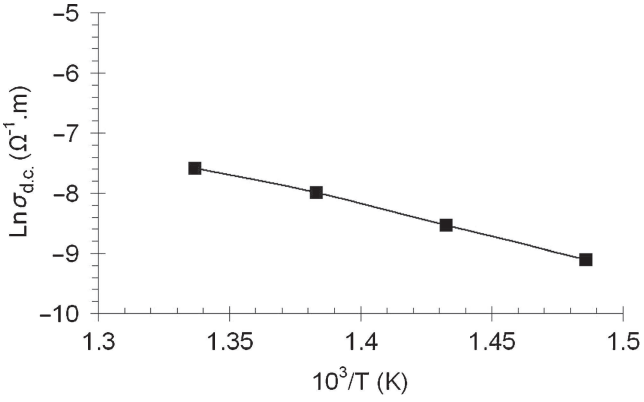

Figure 9. Variation of ln $\sigma_{d.c.}$ with $10^3/T$.

onto a new site from its original position, it remains in a state of displacement between two potential energy minima, which includes contributions from other mobile defects after sufficient time, the defect could relax until the two minima in lattice potential energy coincide with the lattice site.

The d.c. (bulk) conductivity, $\sigma_{d.c.}$, of the sample has been evaluated from the impedance spectrum using the relation $\sigma_{d.c.} = t/AR_b$ where R_b is the bulk resistance (obtained from the intercept of the semicircular arcs Z'' on the real axis (Z')), t the thickness and A the surface area of the sample. Figure 9 shows the variation of ln $\sigma_{d.c.}$ with $10^3/T$. It is observed that $\sigma_{d.c.}$ increases with the increase in temperature further confirming the NTCR behaviour. The nature of variation is linear and follows the Arrhenius relationship:

$$\sigma_{d.c.} = \sigma_0 \exp(E_a/k_B T), \tag{12}$$

where E_a is the activation energy of conduction and T the absolute temperature. The value of activation energy (E_a) as calculated from the slope of ln $\sigma_{d.c.}$ with $10^3/T$ curve is found to be $0.88E_v$. This obtained value indicates that the conduction mechanism in NBTS system may be due to the polaron hopping based on electron carriers, the near value was also funded in $Ba(Zn_{1/2}W_{1/2})O_3$ perovskite.[27] Figure 10 shows

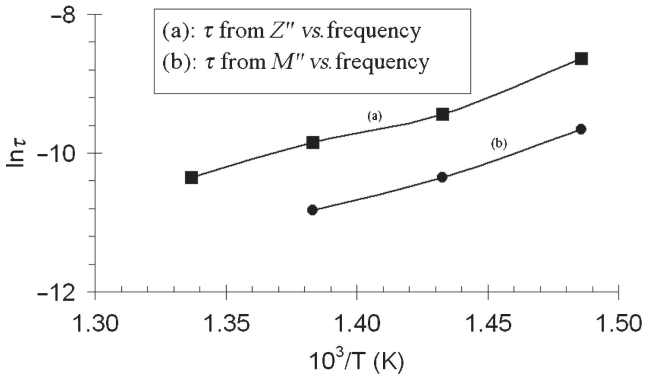

Figure 10. Arrhenius diagram of relaxation times, ln($\tau_{Z''}$) and ln($\tau_{M''}$) as a function of reciprocal temperature.

the variation of relaxation time (ln τ) with inverse of absolute temperature ($10^3/T$). The characteristic relaxation time (τ) was calculated from Z'' and M'' *vs.* frequency plots using the relation: $\tau = 1/\omega = 1/2\pi f_{max}$ where f_{max} is the relaxation frequency (frequency at which Z'' or M'' was found to be maximum).

The logarithmic of the relaxation times derived from Z'' *vs.* frequency and M'' *vs.* frequency functions, as a function of reciprocal temperature $1/T$ are shown in figure 10. The data are described by Arrhenius' expression

$$\tau_{Z''} = \tau_{0Z''} \exp(E_{a_1}/k_B T), \tag{13}$$

$$\tau_{M''} = \tau_{0M''} \exp(E_{a_2}/k_B T), \tag{14}$$

where E_{a_1} and E_{a_2} are the activation energies for the conduction relaxation derived from $Z''(f)$ and $M''(f)$ functions, where $\tau_{0Z''}$ and to $\tau_{0M''}$ are the pre-exponential factor or characteristic relaxation time constants, respectively.

An near value for E_{a1} and E_{a2} is observed on the entire range of temperature measurements being equals to 0.96 and 0.97 eV, respectively. This value of E_a is approximately the same as the energy required (1 eV) for motion of oxygen vacancies.[28] This confirms that the observed conductivity is due to the movements of oxygen vacancies in the material.

5. Conclusions

Polycrystalline $(Na_{0.5}Bi_{0.5})_{0.94}Ba_{0.06}TiO_3 + 0.3$ wt% $Sm_2O_3 +$ 0.25 wt% LiF, prepared through a high-temperature solid-state reaction technique, was found to have a single-phase perovskite-type. Impedance analyses indicated the presence of grain effect in NBTS + 0.25 wt% LiF ceramics. Sample showed dielectric relaxation which is found to be of non-Debye type and the relaxation frequency shifted to higher side with the increase of temperature. The Nyquist plot and conductivity studies showed the NTCR character of NBTS + 0.25 wt% LiF. The frequency-dependent a.c. conductivity at different temperatures indicated that the conduction process is thermally activated process. The activation energy (E_a) of the compound under investigation is calculated using the Arrhenius expression (derived from $Z''(f)$

and $M''(f)$ functions). The value of activation energy (E_a) as calculated from the slope is found to near 1 eV, this value is due to the movements of oxygen vacancy in the material.

References

1. Jaffe B, Cook W R and Jaffe H 1971 *Piezoelectric ceramics* (New York: Academic Press)
2. Yang Z, Chao X and Yang L 2007 *Jpn. J. Appl. Phys.* **46** 6746
3. Takenaka T, Maruyama K and Sakata K 1991 *Jpn. J. Appl. Phys.* **30** 2236
4. Chen M, Xu Q, Kim B H, Ahn B K *et al* 2008 *J. Eur. Ceram. Soc.* **28** 843
5. Fu P, Xu Z, Chu R, Li W, Zang G and Hao J 2010 *Mater. Chem. Phys.* **124** 1065
6. You H W and Koh J H 2006 *Jpn. J. Appl. Phys.* **45** 6362
7. Hu T, Jantunen H, Uusimaki A and Leppavuori S 2003 *Mater. Sci. Semicond. Process.* **5** 215
8. Lee H R, Yoon K H and Kim E S 2003 *Jpn. J. Appl. Phys.* **42** 6168
9. Kim S H and Koh J H 2008 *J. Eur. Ceram. Soc.* **28** 2969
10. Goda K and Kuwabara M 1991 *Ceram. Trans.* **22** 503
11. Bidault O, Goux P, Kchikech M, Belkaoumi M and Maglione M 1994 *Phys. Rev. B* **49** 7868
12. Li W, Chen A P, Lu X U and Zhu J S 2005 *J. Appl. Phys.* **98** 024109
13. Ang C, Yu Z and Cross L E 2000 *Phys. Rev. B* **62** 228
14. Archana S, Choudhary R N P and Thakur A K 2009 *J. Phys. Chem. Solids* **70** 1401
15. Soma D, Choudhary R N P and Sinha P K 2007 *Ceram. Int.* **33** 13
16. Dygas J R, Fafilek G and Breiter M W 1999 *Solid State Ionics* **119** 115
17. Uchino K and Nomura S 1982 *Ferroelectr. Lett.* **44** 55
18. Pilgrim S M, Sutherland A E and Winzer S R 1990 *J. Am. Ceram. Soc.* **73** 3122
19. Prasad K 2000 *Indian J. Eng. Mater. Sci.* **7** 446
20. Barik S K, Choudhary R N P and Mahapatra P K 2007 *Appl. Phys. A* **88** 217
21. Kumar A, Singh B P, Choudhary R N P and Thakur A K 2006 *Mater. Chem. Phys.* **99** 150
22. Choudhary R N P, Pradhan D K, Tirado C M, Bonilla G E and Katiyar R S 2007 *Physica B* **393** 31
23. Suman C K, Prasad K and Choudhary R N P 2005 *Adv. Appl. Ceram.* **104** 294
24. Suman C K, Prasad K and Choudhary R N P 2006 *J. Mater. Sci.* **41** 369
25. Kroger F A and Vink H 1956 *J. Solid State Phys.* **3** 307
26. Jonscher A K 1977 *Nature* **267** 673
27. Ved P, Dutta A, Choudhary S N and Sinha T P 2007 *Mater. Sci. Eng. B* **142** 98
28. Sen S, Choudhary R N P and Pramanik P 2007 *Physica B* **387** 56